

Thermal stability of a Ti-Si-N diffusion barrier in contact with a Ti adhesion layer for Au metallization

I. Shalish^{a)} and Yoram Shapira

Department of Physical Electronics, Tel-Aviv University, Ramat-Aviv, Tel-Aviv 69978, Israel

(Received 19 June 1998; accepted 5 October 1998)

Depth profiling by backscattering spectrometry, x-ray photoelectron spectroscopy and diffractometry, scanning electron microscopy, and sheet resistance measurements were used to study the thermal stability of ternary $\text{Ti}_{27}\text{Si}_{20}\text{N}_{53}$ films as diffusion barriers between a gold overlayer and substrates of aluminum nitride, silicon oxide, and β -silicon carbide when thin titanium films are added on either side of the barrier to enhance adhesion. It is shown that titanium and gold interdiffuse upon 30 min annealing in vacuum at 400 °C and above, which raises the sheet resistance of the gold layer by factors that increase with the amount of titanium present. For the same annealing ambient and duration, nitrogen begins to diffuse at 600 °C from the $\text{Ti}_{27}\text{Si}_{20}\text{N}_{53}$ layer into the titanium layer, releasing silicon. This silicon reacts eutectoidally with the gold, leading to breakup of the barrier. © 1999 American Vacuum Society. [S0734-211X(99)00301-7]

I. INTRODUCTION

Ti-Si-N belongs to a class of ternary films of the type TM-Si-N (TM=Ti, Ta, Mo or W). These films stand out by their excellent performance as barrier materials, preventing the interdiffusion or reaction between Al, Cu or Au and Si.¹⁻¹² For example, a 100-nm-thick Ti-Si-N film effectively blocks the interdiffusion between Si and Cu up to 850 °C for a 30 min annealing in vacuum.⁹ However, chemical inertness is often associated with poor adhesion. It is therefore common practice to include a layer of a reactive element, e.g., Ti, to promote the adhesion of a metal film to an inert substrate or layer, such as SiO_2 or Si_3N_4 , in the belief that a reaction with these materials favors good adhesion. An attempt was also made to achieve good adhesion of a WN_x barrier with an Al overlayer by introducing a Ti film.¹³ However, it was found that the Ti layer reduces WN_x to W upon annealing to 550 °C and that this reaction promotes Al diffusion into W. Thus, it is important to clarify to what extent thin films of reactive metals, such as Ti, actually improve or degrade the performance of a barrier layer.

In this article we examine the thermal stability of a $\text{Ti}_{27}\text{Si}_{20}\text{N}_{53}$ barrier layer with adjoining layers of Ti between a Au overlayer and substrates of AlN, SiO_2 , and β -SiC. The results are similar for all three substrates. We present only the data for AlN. The particular choice of the barrier composition $\text{Ti}_{27}\text{Si}_{20}\text{N}_{53}$ for this study was suggested by the results of Sun *et al.*,¹² where it is shown that the optimum composition range for a conducting, yet atomically opaque, Ti-Si-N barrier is near that composition.

II. EXPERIMENTAL PROCEDURES

A. Sample preparation

Polished AlN plates with a surface roughness of less than 20 nm obtained from The Carborundum Company were used as substrates. The substrates were cut into 8 mm×8 mm

pieces, degreased in organic solvents in an ultrasonic bath (trichloroethylene, acetone, and methanol sequentially) followed by 10 s of a water-diluted HF etch before being loaded into the deposition chamber.

All the films in this study were deposited by rf sputtering with a planar magnetron cathode 7.5 cm in diameter. The substrate plate was placed 7 cm below the target and was neither cooled nor heated externally. The sputtering system is equipped with a cryopump and a cryogenic baffle that provides a background pressure of 4×10^{-7} Torr before sputter deposition. The different layers were deposited sequentially in the same chamber without breaking vacuum. They were all deposited at 10 mTorr total pressure, 300 W rms forward sputtering power and without dc substrate bias. The Ti layers and the Au overlayers were deposited in Ar discharges. Ti-Si-N films were deposited from a Ti_5Si_3 target in Ar/ N_2 gas mixture discharges. The flow ratio of N_2 to Ar (0.036) and the total gas pressure (10 mTorr) were adjusted by mass flow controllers and monitored by a capacitive manometer in a feedback loop.

Four sets of samples of the configuration AlN/Ti/ $\text{Ti}_{27\pm 2}\text{Si}_{20\pm 1}\text{N}_{53\pm 4}$ /Ti(*x*)/Au were prepared. The Ti adhesion layer between the Ti-Si-N and the AlN substrate was 20 nm thick for all sets. The thicknesses of the other adhesion layer [denoted Ti(*x*)] between the Ti-Si-N and the Au were set at 10, 20, 30, and 40 nm with the intention of finding the thickness that would optimize both adhesion and stability. The thicknesses of the Ti-Si-N barrier layer (100 nm) and the Au overlayer (230 nm) were identical for all sets. One sample of each thickness group was kept as a reference. Other samples of each group were annealed for 30 min at one of seven temperatures (400, 500, 600, 700, 750, 800 or 850 °C) in an evacuated tube furnace (5×10^{-7} Torr). To eliminate a possible role of the substrate, the same sequence of layers with Ti(*x*)=20 nm was also deposited on thermally oxidized Si and on β -SiC samples.

To study nitrogen diffusion, a set of four <111> Si substrates covered with thermally grown SiO_2 were degreased

^{a)}Electronic mail: shalish@eng.tau.ac.il

with organic solvents in an ultrasonic bath and sputter deposited under the same conditions described above. A 125-nm-thick Ti layer was deposited on the SiO_2 and subsequently covered with a 100-nm-thick Ti-Si-N overlayer. One of these was kept as a reference, while the others were annealed for 30 min in vacuum at 500, 600, and 700 °C.

B. Sample characterization

Before and after thermal annealing, the samples were characterized by 2.0 MeV $^4\text{He}^{++}$ backscattering spectrometry (BS) to determine the atomic composition profiles and to monitor the interdiffusion or reactions in the samples. Debye–Scherrer x-ray diffractometry with a glancing angle of beam incidence (10°), Co $K\alpha$ radiation ($\lambda=1.79 \text{ \AA}$), and an Inel position-sensitive detector was used for phase identification. Scanning electron microscopy (SEM) and energy dispersive analysis of x rays (EDAX) were used on selected samples to examine surface morphology and to obtain chemical information.

The redistribution of nitrogen in the $\langle\text{Si}\rangle/\text{SiO}_2/\text{Ti}/\text{Ti}_{27\pm 2}\text{Si}_{20\pm 1}\text{N}_{53\pm 4}$ structure upon thermal treatment was tracked by x-ray photoelectron spectroscopy (XPS) or electron spectroscopy for chemical analysis (ESCA) combined with depth profiling. The measurements were carried out in ultrahigh vacuum (3×10^{-10} Torr) using a Phi 5600 multi-technique system with a spherical capacitance analyzer and a monochromatized Al $K\alpha$ radiation ($h\nu=1486.6 \text{ eV}$) source using a spectrometer pass energy of 117 eV with an energy interval of 0.50 eV. Sputtering was done with 4 keV Ar ions at a beam current of 1 μA . Each sputtering cycle lasted 1 min, except for the first 12 cycles where a longer duration, 5 min, was used. To improve the uniformity of layer removal, the samples were rotated during Ar irradiation and the ion beam was rastered over an area of $3 \times 3 \text{ mm}^2$. Photoelectron spectra were acquired over a 400- μm -diam spot in alternation with the sputtering.

The compositions of the Ti-Si-N layers were calculated from the relative signal heights of the elements in the backscattering spectra of the same films on graphite substrates. The as-deposited $\text{Ti}_{27}\text{Si}_{20}\text{N}_{53}$ films also generally contained 2 at. % Ar and 4–6 at. % oxygen. The thicknesses of single element layers were estimated with a typical error of $\pm 7\%$ from elemental bulk densities and energy losses in the backscattering spectra. The thickness of the Ti-Si-N layers was determined from a cross-sectional SEM micrograph of a typical sample, whereas the other samples were compared with the SEM sample using energy losses in the backscattering spectra.

III. RESULTS

A. X-ray photoelectron spectroscopy

Figure 1 shows the evolution of the $\text{N}(1s)$ peak versus sputtering cycle and binding energy for an as-deposited $\langle\text{Si}\rangle/\text{SiO}_2/\text{Ti}/\text{Ti}_{27}\text{Si}_{20}\text{N}_{53}$ sample and samples of the same layer scheme annealed in vacuum ($<5 \times 10^{-7}$ Torr) at 500, 600, and 700 °C for 30 min. A redistribution of the nitrogen

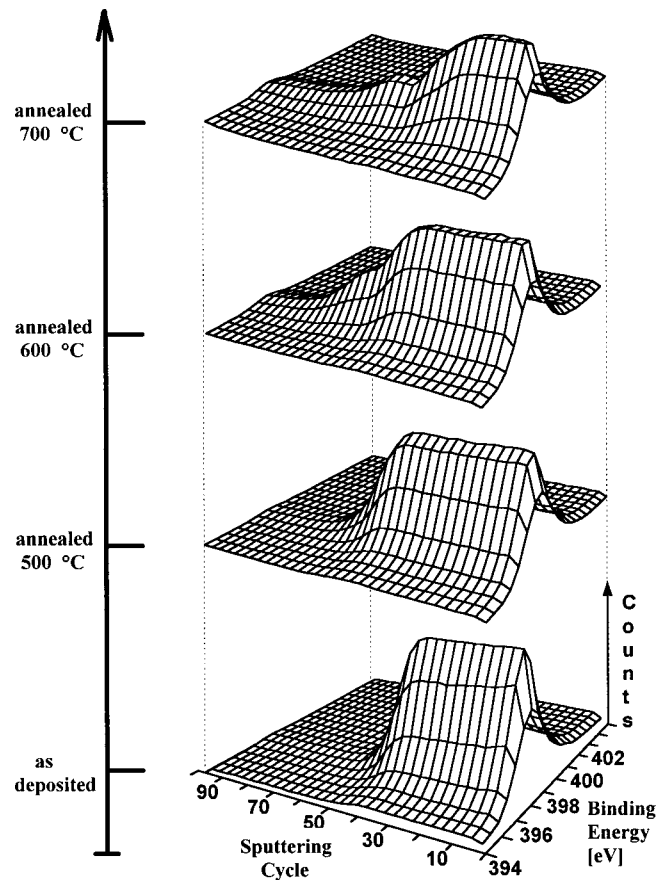


FIG. 1. Evolution of x-ray photoelectron spectra of $\text{N}(1s)$ vs sputtering cycle for four $\langle\text{Si}\rangle/\text{SiO}_2/\text{Ti}/\text{TiSiN}$ samples: as deposited, and annealed in vacuum for 30 min at 500, 600, and 700 °C. The 100 sputtering cycles shown correspond to the depth of the two topmost layers, Ti (125 nm)/TiSiN (100 nm).

is observed starting at 600 °C and increasing with the annealing temperature. A sharp drop of the $\text{N}(1s)$ peak in the as-deposited sample indicates the transition from the top $\text{Ti}_{27}\text{Si}_{20}\text{N}_{53}$ layer to the underlying Ti layer. Nitrogen is uniformly distributed throughout the $\text{Ti}_{27}\text{Si}_{20}\text{N}_{53}$ layer and is below XPS resolution in the Ti layer. No significant change is observed after annealing at 500 °C (similar changes in the top layer thickness were observed in the depth profiles of Ti and Si, eliminating the possibility of diffusion at this temperature). At 600 °C, the $\text{N}(1s)$ peak in the Ti layer increases close to the interface, along with a corresponding lowering of the peak in the $\text{Ti}_{27}\text{Si}_{20}\text{N}_{53}$ layer. The extent of this change grows with annealing temperature.

The penetration of nitrogen into the Ti layer is accompanied by a consequent release of Si from the Ti-Si-N layer close to the interface. Figure 2 shows the evolution of the $\text{Si}(2p)$ peak with the sputtering cycle for the same set of samples as in Fig. 1. In the spectra of the as-deposited sample, the $\text{Si}(2p)$ peak is observed at a binding energy (BE) of 102.1 eV throughout the Ti-Si-N layer. This BE is within the reported range for silicon nitrides (101.5–102.2 eV).¹⁴ At the interface with the Ti layer, an additional relatively weak peak is noticed at BE of 99.3 eV, typical of pure

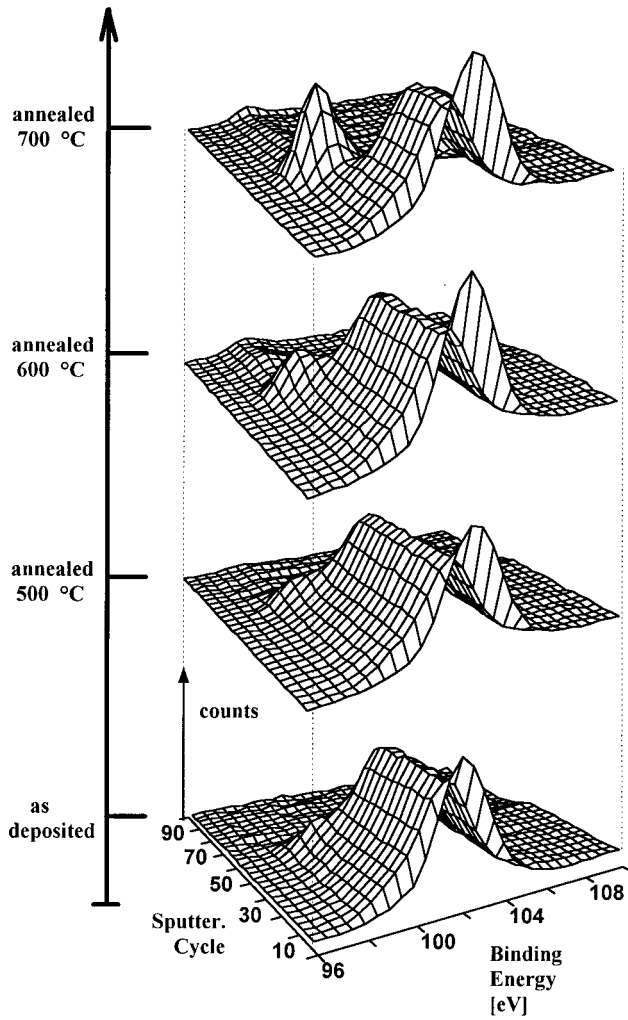


FIG. 2. Evolution of x-ray photoelectron spectra of Si($2p$) vs sputtering cycle for four (Si)/SiO₂/Ti/TiSiN samples: as-deposited, and annealed in vacuum for 30 min at 500, 600, and 700 °C. The 100 sputtering cycles shown correspond to the depth of the two topmost layers, Ti (125 nm)/TiSiN(100 nm).

Si (98.8–99.4 eV).¹⁴ An increase of this pure Si peak is observed only after annealing at 600 °C, and is made prominent after annealing at 700 °C.

A reaction also takes place between the Ti layer and the SiO₂ substrate. It is noticed starting at 600 °C as a minor diffusion of Si from the SiO₂ into the Ti layer. This reaction is known to occur at about 600 °C.¹⁵ However, this reaction yields TiO₂ and TiSi_x, and therefore it is unlikely to take part in the development of the pure Si peak.

In order to identify phases in the Ti₂₇Si₂₀N₅₃ layer, Ti($2p_{3/2}$) and Si($2p$) peaks were analyzed for a sequence of 10 sputtering cycles around the center of this layer. The resulting parameters were averaged. The Ti($2p_{3/2}$) peak in the as-deposited Ti-Si-N layer comprises two Gaussian peaks in a typical satellite arrangement. The main peak appears at BE of 455.1 eV (standard deviations of less than 0.1 eV are omitted), matching reported values in TiN₁,^{14,16} while the satellite peak appears at BE of 457.0 ± 0.2 eV. The Si($2p$) peak resolves into three Gaussian components. The

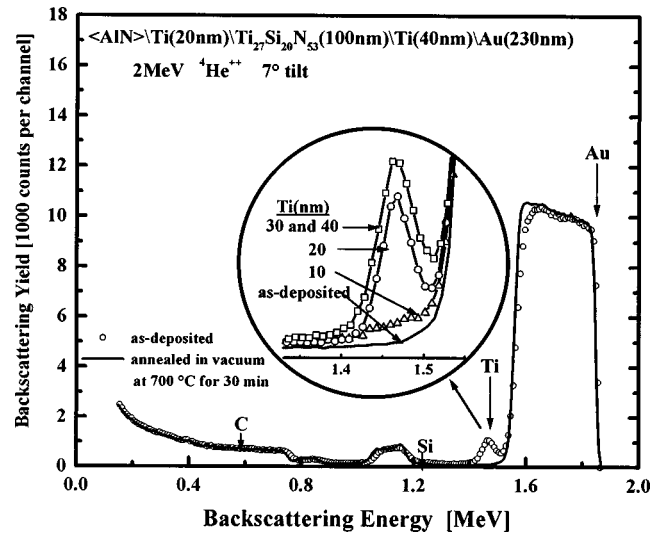


FIG. 3. 2 MeV $^4\text{He}^{++}$ backscattering spectra of the second group AlN/Ti (20 nm)/Ti₂₇Si₂₀N₅₃ (100 nm)/Ti (40 nm)/Au (230 nm) before and after annealing at 700 °C. After annealing an additional Au peak occurs in the spectrum just below the low-energy edge of the Au signal. The change of its intensity according to the thickness of the Ti(x) layer is displayed in the zoomed circle.

main component is centered at BE of 101.6 eV, typical of Si₃N₄,¹⁴ while the two minor components are centered at 99.3 ± 0.1 eV, typical of pure Si,¹⁴ and 102.4 ± 0.4 eV, attributed to Si₃N₂O.¹⁷ The full width at half maximum (FWHM) of the Ti($2p_{3/2}$) in the Ti-Si-N layer is 1.4 eV, in agreement with reported values for TiN₁,¹⁸ while the FWHM of the Si₃N₄ component of Si($2p$) is 2.0 eV, which is much wider compared to reported values for crystalline Si₃N₄.¹⁹ The changes of the above listed parameters after annealing at various temperatures are below measurement resolution. These results indicate that Ti₂₇Si₂₀N₅₃ is composed mainly of crystalline TiN and less ordered Si₃N₄, as well as small quantities of Si and Si₃N₂O, and that this composition does not change upon annealing in vacuum up to 700 °C.

B. Backscattering spectrometry

Two types of interactions involving the Au layer were observed by backscattering. One type is an apparent interaction between the Ti(x) layer and its overlying Au layer. It is evidenced by a smearing of the high-energy edge of the Ti signal in spectra of the annealed samples. Corresponding changes in the Au signal are observed as well but are more pronounced in spectra of thick Ti(x) layer samples. The change consists of a slight lowering of the Au signal, mostly at its low-energy edge.

A second type of interaction is observed after annealing at temperatures above 600 °C. It is evident as a new peak appearing just below the low-energy edge of the Au signal. Initial changes of this type appear on samples with Ti(x) = 30 and 40 nm after annealing at 600 °C. Annealing at 700 and 750 °C produces this change in all the samples. Figure 3, for example, displays 2 MeV $^4\text{He}^{++}$ backscattering spectra of the sample with Ti(x) = 40 nm before and after annealing

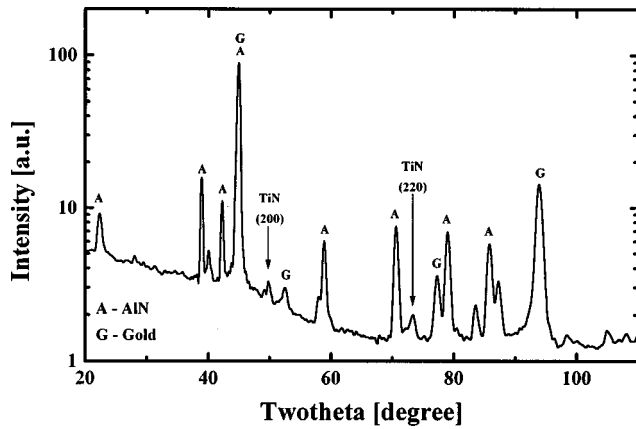


FIG. 4. 15° glancing angle x-ray diffraction (Co $K\alpha$) spectrum of an as-deposited AlN/Ti/TiSiN/Ti/Au sample.

at 700 °C. A peak just below the low-energy edge of the Au signal appears, by coincidence, at the surface energy of Ti. Backscattering from the same sample tilted against the incident beam showed a shift of this peak to lower energies, identifying it as Au. The depth of this additional Au peak was calculated to be located approximately under the $Ti_{27}Si_{20}N_{53}$ layer, suggesting that some Au diffuses through that layer during annealing. The $Ti_{27}Si_{20}N_{53}$ layer itself is still identifiable as a distinct entity after the 700 °C annealing, as the Ti signal between 1.1 and 1.2 MeV attests to. The inset in Fig. 3 compares the intensity of the additional Au peak for the various $Ti(x)$ layer thicknesses. The intensity increases with the thickness of the $Ti(x)$ layer.

C. X-ray diffraction

TiN(200) and TiN(220) peaks were identified in x-ray diffraction spectra of as-deposited samples, together with peaks of Au and hexagonal AlN (Fig. 4). No difference was observed between samples of various $Ti(x)$ thicknesses. Polycrystalline TiN is commonly observed in the (111) preferred orientation. However, a high flow of nitrogen during growth is known to switch the orientation to (200),^{20,21} which may well be the case for our Ti-Si-N layer (53 at. % nitrogen).

D. Scanning electron microscopy

The surfaces of the samples were examined with a scanning electron microscope before and after annealing. Up to 750 °C the continuity of the Au layer is preserved, although the formation of hillocks and holes is observed as well (Fig. 5). These are commonly observed on surfaces of heat treated Ti/Au metallizations and are usually ascribed to relief of stresses resulting from different thermal expansion coefficients.²² Solidified Au droplets were observed on the surface of the samples after annealing at 800 °C or above. Droplet formation was observed *only* in samples incorporating a $Ti(x)$ layer. Figure 6(a) shows Au droplets formed on a sample with $Ti(x)=10$ nm upon annealing in vacuum at 800 °C for 30 min. The positive contact angle of the droplet [Fig. 6(b)] eliminates solid state dewetting as a possible

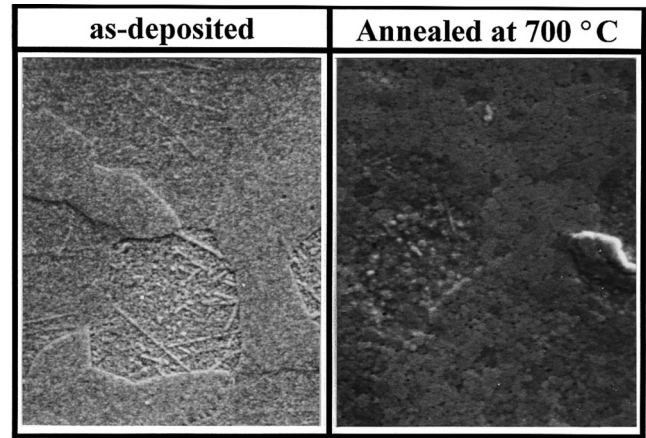


FIG. 5. SEM micrograph of the surface of an AlN/Ti/TiSiN/Ti/Au sample with $Ti(x)=30$ nm before and after 30 min annealing at 700 °C.

cause. The composition of the center of the droplet was examined by EDAX and was found to consist mainly of Au, whereas Si and Au were the main constituents in the border areas of the droplet. Annealing of a sample from the same group at 850 °C results in a similar droplet picture. However, each of the droplets is now surrounded with distinct margins [Fig. 7(a)]. Si and Au were detected by EDAX at these margins [Fig. 7(b)]. A cross-sectional micrograph of the same annealed sample (Fig. 8) reveals a columnar structure of the Ti-Si-N layer with a lateral period of about 60 nm.

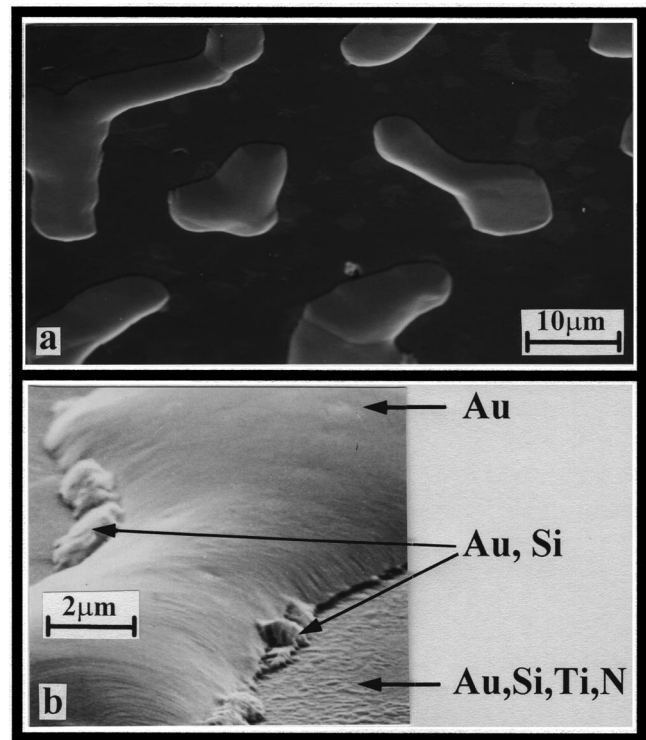


FIG. 6. SEM micrograph of droplets formed on a sample with $Ti(x)=10$ nm upon 30 min of annealing at 800 °C (a) and the composition of one droplet (b).

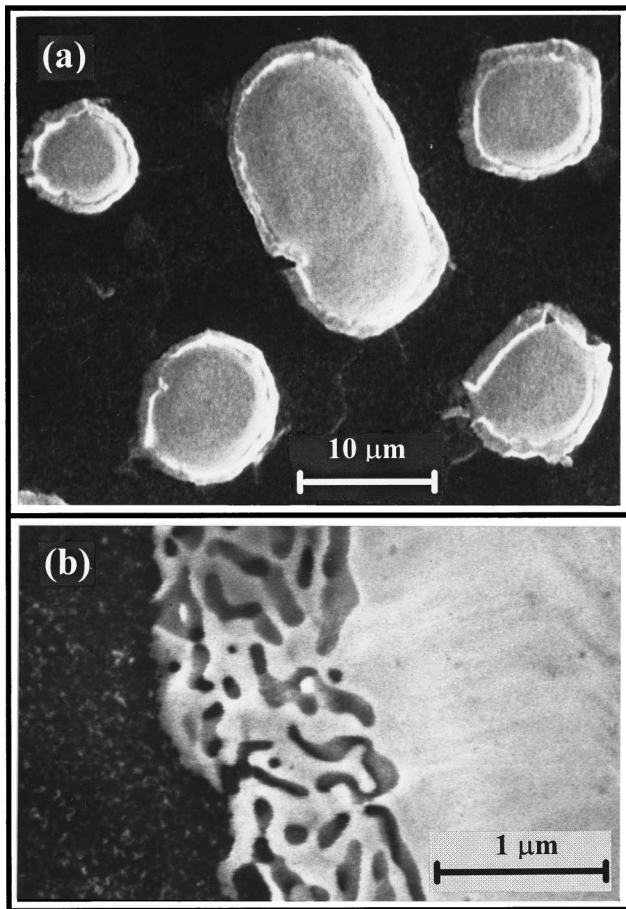


FIG. 7. SEM micrograph of droplets formed on a sample with Ti(x) = 10 nm upon 30 min of annealing at 850 °C (a) and of the margins of a droplet (b).

E. Sheet resistance

The sheet resistance of $0.40 \pm 0.01 \Omega/\square$ measured on the as-deposited samples does not show any dependence on the Ti(x) layer thickness. Values from different as-deposited samples vary insignificantly within the experimental error. This means that layers other than the top Au layer do not affect the sheet resistance of as-deposited samples. The same conclusion may be reached by comparing the sheet resistances [$0.1 \Omega/\square$ for Au, $10.4 \Omega/\square$ for Ti (40 nm), and 11–180 Ω/\square for Ti-Si-N] of the various layers expected from their thicknesses and the respective bulk resist-

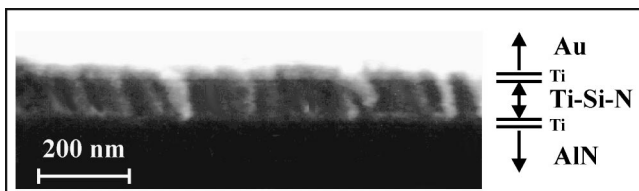


FIG. 8. SEM micrograph of a cross section of an AlN/Ti/TiSiN/Ti/Au sample showing a columnar structure of the $\text{Ti}_{27}\text{Si}_{20}\text{N}_{53}$ barrier layer.

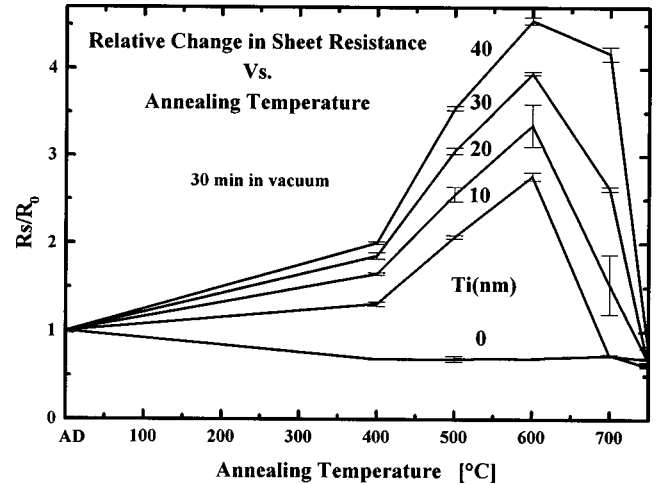


FIG. 9. Relative changes in sheet resistance vs annealing temperature for different thicknesses of Ti.

ivities [$\rho_{\text{Au}} = 2.2 \mu\Omega \text{ cm}$, $\rho_{\text{Ti}} = 41.67 \mu\Omega \text{ cm}$,²³ $\rho_{\text{Ti-Si-N}} = 110/1800 \mu\Omega \text{ cm}^{24}$]. In the case of the annealed samples, shown previously, interactions between layers change their composition. The dominance of the overall conductance by the Au layer (by factors of 100 and 1000) over these of Ti(x) and $\text{Ti}_{27}\text{Si}_{20}\text{N}_{53}$ is so large, however, that one can safely ignore the presence of the latter even after interaction between the layers. We therefore assume that the measured sheet resistance values reflect the sheet resistance of the top Au layer.

The initial resistivity of the Au overlayer in all the as-deposited samples, calculated from the sheet resistance and the Au thickness, is $(9.2 \pm 0.2) \mu\Omega \text{ cm}$. This value is over four times that of pure Au ($2.2 \mu\Omega \text{ cm}$). In a consecutive experiment, we have found that by using a lower Ar pressure during the Au layer deposition (3 instead of the 10 mTorr mentioned in Sec. II A) results in films with resistivities of only 1.8 times that of pure Au as well as a lower content of Ar. It is commonly observed that thin films have significantly higher resistances than bulk samples of the same material, for various reasons.^{25,26}

The relative change in the sheet resistance of the annealed samples with respect to their as-deposited values is given in Fig. 9 as a function of the annealing temperature. Each data point represents a distinct sample annealed to only one temperature. All samples annealed at temperatures below 750 °C show an increase in their sheet resistance. For the same temperature the increase is higher for thicker Ti(x) layers. This increase reaches its maximum value at 600 °C (2.5–4.5 times the initial value). Annealing at 700 °C results in a value that is less than that a maximum, and after 750 °C the sheet resistance falls below its initial value. The values at 750 °C do not show a dependence on the Ti(x) thickness and vary around a value that is about 60% of the initial (as-deposited) value.

IV. DISCUSSION

Two major opposing trends characterize the changes in sheet resistance after annealing (seen in Fig. 9). One, already effective at low temperatures, increases the resistance with annealing temperature. The other sets in somewhat below 600 °C and opposes the first. Their superposition results in a maximum at 600 °C. At 750 °C the two trends cancel each other. The role of Ti is evident through the correlation between the Ti(x) layer thickness and the magnitude of the sheet resistance increase after annealing. If the presence of Ti is solely responsible for that increase, then no such increase should be expected in its absence. Confirmation of that is indeed found in the Ti(x)=0 curve in Fig. 9.

The resistance of thin films is sensitive to contamination.²⁶ In our case, the measured layer is Au, into which contaminants can penetrate either from its underlayer or from the ambient. As the latter is not evident in backscattering spectra, it seems reasonable to assume that an interaction of the Au layer with the underlying Ti(x) is the main cause of the observed changes. Hence, the extent to which the resistance increases should be expected to correlate with the quantity of Ti that penetrates the Au. This in turn should depend on the original quantity of Ti [Ti(x) thickness] minus the part of Ti lost for concurrent reactions. Other than with Au, Ti(x) may react with the other adjoining layer, Ti-Si-N. These two reactions will therefore be discussed next.

The Ti-Au reaction has been at the focus of several studies.^{22,27–35} In most of these it is found that Ti reacts with both the substrate and the ambient as well as with Au. Vacuum annealings were used by Poate *et al.*²⁹ and by Hieber.³¹ In general, when the Au layer is thicker than the underlying Ti layer, Ti diffuses into Au faster than vice versa, producing Au-rich compounds. Hieber shows that the sheet resistance of a Ti (50 nm)/Au (500 nm) bilayer first decreases upon annealing to about 60% of its initial value due to Au recovery. A following increase of sheet resistance is found to correlate with the onset of Ti-Au reaction at 207 °C.³¹ A decrease to about 60% of the initial value is also observed in the present work when the Ti(x) layer is absent [Ti(x)=0]. An evident correlation of that decrease with a narrowing of the Au peaks seen by x-ray diffraction suggests Au grain growth as a plausible cause. For Ti(x)>0 Ti-Au interaction in the annealed samples is observed by backscattering (see, for example, Fig. 3). On the other hand, no conclusive evidence for the presence of Ti-Au phases is found in XRD spectra, possibly because of the limited amount of Ti(x). These findings indicate that, when a Ti(x) layer is present between the Au and the Ti-Si-N layers, the increase in the Au sheet resistance upon annealing is caused by Ti penetrating the Au layer.

At temperatures equal to or higher than 600 °C, the Ti-Au reaction is no longer exclusive since concurrent reactions take place. Evidence of Ti interaction with the Ti-Si-N barrier layer is provided by the XPS depth profiles in Figs. 1 and 2. Nitrogen diffusion from the Ti-Si-N layer to the adjoining Ti layer is first observed after annealing at 600 °C. That is

the same temperature (600 °C) at which the sheet resistance peaks. Although the Au layer has reacted with the Ti(x) films at the lower temperatures, we surmise from the concurrence of the two phenomena that a similar process takes place here too. Heat of formation values for all constituents are unavailable, but it is plausible that TiN plus Au-Si formation is favored over Ti-Au phases and Ti-Si-N. A reaction between Ti and Ti-Si-N is also supported by the Ti-Si-N ternary phase diagram, where no tie lines exist between Ti and TiN or Si₃N₄.³⁶ Assuming that the formation of the Ti-Au phases can be reversed, the sheet resistance at 750 °C should be expected to be roughly similar for samples with or without a Ti(x) layer. This is indeed seen in Fig. 9. In the absence of Ti-Au reaction, the most probable mechanism available that would influence the sheet resistance would be Au grain growth. Narrowing of the Au peaks in x-ray diffraction spectra was indeed observed after annealing, providing some support for that possibility, although several other effects could also result in such narrowing.³⁷

At 800 °C, a new phenomenon is observed. Solidified Au droplets, evident by SEM after annealing at 800 and 850 °C [Figs. 6(a) and 7(a) for Ti(x) of 10 nm], suggest that a eutectic reaction involving Au occurs. The only possible eutectic up to 850 °C is that of Si and Au at 363±3 °C.³⁸ Si, identified by EDAX at the margins of these droplets [Figs. 6(b) and 7(b)], supports this possibility. This Si must originate from the Ti-Si-N layer. The reaction of Ti with Ti₂₇Si₂₀N₅₃ indicates that Si becomes available to react with Au only above 600 °C. Therefore, it is likely that the formation of the Si-Au eutectic and of the Ti-N phases is dominated by grain boundary processes, which are local and proceed at locally varying rates. Ultimately, the Ti₂₇Si₂₀N₅₃ barrier fails locally, and allows penetration of Au below the barrier, as was observed by backscattering at temperatures of 600–750 °C. Only a local process can be consistent with these backscattering spectra. The result of Fig. 6 would presumably occur at temperatures lower than 800 °C for annealing durations longer than 30 min.

A columnar structure, as observed in Fig. 8, may explain the local nature of the reaction. According to Sun *et al.*, Ti-Si-N favors a structure composed of TiN-like nanograins embedded in a Si₃N₄-like amorphous material. This means that TiN and Si₃N₄ phases segregate during the formation of Ti-Si-N. Order and crystallinity have been found to increase with nitrogen concentration. Columnar grain structure, typical of TiN, was observed in the case where the nitrogen concentration was the highest (Ti₃₅Si₁₃N₅₂). Nevertheless, this layer was found to prevent the interdiffusion of Cu and SiO₂ up to 30 min of annealing at 850 °C.¹² The composition Ti₂₇Si₂₀N₅₃ used in this work is also very close to the TiN-Si₃N₄ tie line in the Ti-Si-N ternary phase diagram,³⁶ and it also shows a columnar grain structure (Fig. 8). X-ray photoelectron spectroscopy of as-deposited samples reveals that Ti in Ti₂₇Si₂₀N₅₃ takes the form of TiN, while Si is mostly found as Si₃N₄ together with some pure Si and oxynitrides. X-ray photoelectron spectroscopy studies of Si₃N₄ have shown a typical Si(2p) FWHM of 1.15 eV for stoichio-

metric Si_3N_4 . The much larger FWHM in our case (2.0 eV) suggests a wide range of possible silicon nitride compositions that could be an expression of chemical and structural disorder in an amorphous material. An amorphous structure could also explain the absence of Si_3N_4 peaks in XRD. Support is also found in other studies of similar Ti-Si-N layers using XRD and transmission electron microscopy. These studies have identified crystalline TiN together with an amorphous component thought to be Si_3N_4 .^{39,40} On the other hand, the TiN in our $\text{Ti}_{27}\text{Si}_{20}\text{N}_{53}$ yields a narrow crystalline peak in XPS, a preferred (200) orientation in XRD, and a columnar grain structure in SEM, all of which are commonly observed in TiN films.⁴¹ However, despite its columnar structure and the similarity to TiN, $\text{Ti}_{27}\text{Si}_{20}\text{N}_{53}$ still seems impenetrable to Au up to at least 800 °C when a Ti(x) layer is absent.⁴² This could suggest that the columnar grain boundaries are initially “stuffed,” presumably with the amorphous Si_3N_4 phase. Alternatively, it could be that Ti only enhances penetration of the barrier by the Au and that penetration might also have been observed without a Ti(x) layer had a longer annealing time been used. In any case, when a Ti(x) layer is present, it getters nitrogen upon annealing, preferably at the grain boundaries, thus reducing some of the Si_3N_4 to Si. The availability of Si between the Ti-Si-N columns encourages Au diffusion between the columns, giving rise to a laterally nonuniform Si-Au reaction and penetration of the barrier.

Our results, together with those of So *et al.*,¹³ provide evidence of the role of (Ti) in the failure of adjoining nitride barrier layers. In both cases, the same mechanism (nitrogen gettering) was identified as the cause of failure, since the nitrogen affinity of Ti is higher than that of the barrier components. This provides a driving force for nitrogen to leave the barrier. The same mechanism may also apply to barrier materials containing a light element other than nitrogen (e.g., borides, phosphides, or oxides) depending on the stability of Ti and the specific components present.

V. CONCLUSION

Use of a thin Ti layer in contact with a 100-nm-thick $\text{Ti}_{27}\text{Si}_{20}\text{N}_{53}$ barrier layer is shown to deleteriously affect the integrity of the barrier layer by way of gettering nitrogen from the barrier. Silicon is then available for a eutectic reaction with the Au overlayer. This reaction sets in at about 600 °C, and has the same effect for all three substrates used (AlN, β -SiC, and SiO_2). The laterally nonuniform degradation of the barrier layer is attributed to a columnar structure of the grains in $\text{Ti}_{27}\text{Si}_{20}\text{N}_{53}$. The finding of columnar grains in $\text{Ti}_{27}\text{Si}_{20}\text{N}_{53}$ adds to existing knowledge in suggesting that Ti-Si-N growth depends on the nitrogen concentration in a way that is rather similar to that of its close relative, TiN.

ACKNOWLEDGMENTS

The authors gratefully acknowledge the technical assistance of R. Gorris and M. Easterbrook of Caltech. They also thank Dr. L. Burstein, Tel-Aviv University, for the XPS measurements.

- ¹K. Onodera, M. Tokumitsu, S. Sugitani, Y. Yamane, and K. Asai, *IEEE Electron Device Lett.* **EDL-9**, 417 (1988).
- ²E. Kolawa, J. M. Molarius, C. W. Nieh, and M.-A. Nicolet, *J. Vac. Sci. Technol. A* **8**, 3006 (1990).
- ³A. Lahav, K. A. Grim, and I. A. Blech, *J. Appl. Phys.* **67**, 734 (1990).
- ⁴A. Tamura, Y. Ikeda, T. Yokoyama, and K. Inoue, *J. Appl. Phys.* **67**, 6171 (1990).
- ⁵P. J. Pokela, E. Kolawa, R. Ruiz, and M.-A. Nicolet, *J. Electrochem. Soc.* **138**, 2125 (1990).
- ⁶E. Kolawa, J. S. Chen, J. S. Reid, P. J. Pokala, and M.-A. Nicolet, *J. Appl. Phys.* **70**, 1369 (1991).
- ⁷U. Merkel, E. Neuyebauer, and M. May, *Thin Solid Films* **217**, 108 (1992).
- ⁸J. S. Reid, E. Kolawa, R. P. Ruiz, and M.-A. Nicolet, *Thin Solid Films* **236**, 319 (1993).
- ⁹J. S. Reid, X. Sun, E. Kolawa, and M.-A. Nicolet, *IEEE Electron Device Lett.* **15**, 298 (1994).
- ¹⁰H. Sinriki, T. Komiya, N. Takeyasu, and T. Ohta, *Jpn. J. Appl. Phys., Part 1* **34**, 992 (1995).
- ¹¹J. S. Reid, E. Kolawa, C. M. Garland, M.-A. Nicolet, F. Cardone, D. Gupta, and R. P. Ruiz, *J. Appl. Phys.* **79**, 1109 (1996).
- ¹²X. Sun, J. S. Reid, E. Kolawa, and M.-A. Nicolet, *J. Appl. Phys.* **81**, 664 (1997).
- ¹³F. C. T. So, E. Kolawa, H. P. Kattelus, X.-A. Zhao, and M.-A. Nicolet, *J. Vac. Sci. Technol. A* **4**, 3078 (1986).
- ¹⁴J. F. Moulder, W. F. Stickle, P. E. Sobol, and K. D. Bomben, *Handbook of X-ray Photoelectron Spectroscopy*, edited by J. Chastain (Perkin-Elmer, Eden Prairie, MN, 1993).
- ¹⁵S.-J. Kim and M.-A. Nicolet, *Proceedings of the 1st Electronic Materials and Processing Congress* (ASM International, Chicago, 1988), pp. 79–94.
- ¹⁶P. Prieto and R. E. Kirby, *J. Vac. Sci. Technol. A* **13**, 2819 (1995).
- ¹⁷R. Van Weeren, E. A. Leone, S. Curran, L. C. Klein, and S. C. Danforth, *J. Am. Ceram. Soc.* **77**, 2699 (1994).
- ¹⁸M. Delfino, J. R. Fair, and D. Hodul, *J. Appl. Phys.* **71**, 6079 (1992).
- ¹⁹C. H. F. Peden, J. W. Rogers, Jr., N. D. Shinn, K. B. Kidd, and K. L. Tsang, *Phys. Rev. B* **47**, 15622 (1993).
- ²⁰W. Xi, L. Xianghuai, C. Youshan, Y. Genqing, Z. Zuyau, Z. Zhihong, H. Wei, and Z. Shichang, *Nucl. Instrum. Methods Phys. Res. B* **59/60**, 272 (1991).
- ²¹H. Jiang, K. Tau, and H. Li, *Thin Solid Films* **258**, 51 (1995).
- ²²J. Y. Kim and R. E. Hummel, *Phys. Status Solidi A* **122**, 255 (1990).
- ²³J. Babiskin, in *American Institute of Physics Handbook*, 2nd ed. edited by D. E. Gray (McGraw-Hill, New York, 1963), pp. 9–42.
- ²⁴X. Sun, J. S. Reid, E. Kolawa, and M.-A. Nicolet, *J. Appl. Phys.* **81**, 656 (1997).
- ²⁵L. I. Meissel and M. H. Francombe, *An Introduction to Thin Films* (Gordon and Breach Science, New York, 1973), pp. 160–168.
- ²⁶P. M. Hall, J. M. Morabito, and J. M. Poate, *Thin Solid Films* **33**, 107 (1976).
- ²⁷T. C. Tisone and J. Drobek, *J. Vac. Sci. Technol.* **9**, 271 (1971).
- ²⁸J. D. Speight and K. Cooper, *Thin Solid Films* **25**, S31 (1975).
- ²⁹J. M. Poate, P. A. Turner, W. J. DeBonte, and J. Yahalom, *J. Appl. Phys.* **46**, 4275 (1975).
- ³⁰R. Audino, G. DeStefanis, F. Gorgellino, E. Pollino, and S. Tamagno, *Thin Solid Films* **36**, 343 (1976).
- ³¹H. Hieber, *Thin Solid Films* **37**, 335 (1976).
- ³²W. D. Sylwesterowicz, H. A. Elkholy, and G. W. Kammelott, *J. Mater. Sci.* **14**, 873 (1979).
- ³³N. G. Dhare and B. K. Patnik, *Thin Solid Films* **85**, 316 (1981).
- ³⁴C. H. Ling, *Phys. Status Solidi A* **80**, K59 (1983).
- ³⁵K. Masahiro and S. Noboru, *J. Mater. Sci.* **28**, 5088 (1993).

- ³⁶S. Sambasivan and W. T. Petuskey, *J. Mater. Res.* **9**, 2362 (1994).
- ³⁷C. S. Barret and T. B. Massalski, *Structure of Metals*, 3rd ed. (McGraw-Hill, New York, 1966), p. 155.
- ³⁸T. B. Massalski, *Binary Alloy Phase Diagrams*, 2nd ed. (ASM International, Metals Park, OH, 1990).
- ³⁹W. Posadowski, *Thin Solid Films* **162**, 111 (1988).
- ⁴⁰T. Iijima, Y. Shimooka, and K. Suguro, *IEICE Trans. Electron.* **E79C**, 568 (1996).
- ⁴¹R. I. Hegde, R. W. Fiordalice, and E. O. Travis, *J. Vac. Sci. Technol. B* **11**, 1287 (1993).
- ⁴²I. Shalish, S. M. Gasser, E. Kolawa, M.-A. Nicolet, and R. P. Ruiz, *Thin Solid Films* **289**, 166 (1996).